

CrossMark
click for updates

Cite this: DOI: 10.1039/c4ta06046f

Highly efficient sulfonated-polystyrene–Cu(II)@Cu₃(BTC)₂ core–shell microsphere catalysts for base-free aerobic oxidation of alcohols†

Xiaowei Zhang, Wenjun Dong, Yi Luan, Mu Yang, Li Tan, Yangguang Guo, Hongyi Gao, Yin Hai Tang, Rui Dang, Jie Li and Ge Wang*

A novel catalyst consisting of a functional sulfonated-polystyrene (SPS) core, a porous Cu₃(BTC)₂ shell and an active Cu(II) interface between the core and shell was developed via a facile step-by-step assembly method. The polystyrene core was sulfonated first to achieve functional –SO₃H groups on its surface. The main function of the –SO₃H groups was to graft Cu(II) ions to generate an active Cu(II) interface, and the excess –SO₃H could provide acid conditions for the catalytic reaction. The Cu(II) interface along with the acid conditions and the co-catalyst 2,2,6,6-tetramethyl-piperidyl-1-oxyl (TEMPO) enhanced the catalytic activity for the aerobic oxidation of alcohols to aldehydes by molecular oxygen under base-free conditions. A portion of Cu(II) ions on the SPS surface was then coordinated with H₃BTC (1,3,5-benzenetricarboxylic acid) to form a porous Cu₃(BTC)₂ shell, which could protect the active metal from leaching as well as provide porous channels for mass transfer, resulting in high stability and recyclability in the catalysis procedure. The SPS–Cu(II)@Cu₃(BTC)₂ catalyst could be recycled ten times without a significant loss in its activity and selectivity. Furthermore, the SPS–Cu(II)@CuBDC (BDC = 1,4-benzenedicarboxylate) composite was also synthesized and showed high efficiency for catalyzing the aerobic oxidation of alcohols and aerobic homocoupling of arylboronic acids, suggesting that the unique nanostructure of SPS–Cu(II)@MOFs can be easily extended to design complex catalysts with high efficiency and good stability for different catalytic reactions.

Received 9th November 2014

Accepted 8th January 2015

DOI: 10.1039/c4ta06046f

www.rsc.org/MaterialsA

1. Introduction

Selective oxidation of alcohols to aldehydes is a vital and common transformation in the synthesis of important intermediates and fine chemicals.^{1–3} Traditionally, stoichiometric oxidants are required to achieve high catalytic efficiency, which are toxic and often produce waste and harmful byproducts.^{4,5} Recently, more sustainable reaction processes with molecular oxygen as an ideal oxidant^{6–8} have attracted significant attention. However, due to the relatively weak oxidizing properties of molecular oxygen, the direct oxidation of alcohols by dioxygen is difficult, and appropriate catalysts are needed to complete the aerobic oxidation process.⁹

Recent investigations have confirmed that noble metals such as palladium,¹⁰ ruthenium^{11,12} and gold¹³ can efficiently and selectively catalyze the oxidation of alcohols with molecular oxygen. However, it is desirable to develop non-noble metal catalysts to promote the catalytic oxidation reaction due to the high cost and complicated synthesis processes of noble metal catalysts. Copper species,^{14,15} as a classical non-noble transition metal, is considered to be one of the most attractive catalysts for the aerobic oxidation of alcohols on account of its abundant resources, low cost, non-toxic properties and high catalytic efficiency. In particular, copper(II) complexes combined with TEMPO^{16,17} have been proved to have good catalytic performance for alcohol oxidation. Until now, many efficient Cu(II)/TEMPO catalytic systems such as Cu(II)-bipyridine/TEMPO,¹⁸ copper(II)/2-*N*-arylpiperidylcarbamidate/TEMPO¹⁹ and CuBr₂/*N*-benzylidene-*N,N*-dimethylethane-1,2-diamine/TEMPO²⁰ have been reported and favorable catalytic activities have been achieved. However, most Cu/TEMPO catalysts often require a large excess of base additives or alkaline ligands to neutralize acid products² or deprotonate the alcohols,^{21,22} which always causes carboxylate product and basic waste disposal problems^{23,24} as well as separation difficulties for catalytic recycling.²⁵ Interestingly, other studies have revealed that some Cu(II) salts can catalyze alcohol oxidation by using TEMPO as a co-catalyst

School of Materials Science and Engineering, University of Science and Technology Beijing, Beijing 100083, China. E-mail: gewang@mater.ustb.edu.cn; Fax: +86-10-62327878; Tel: +86-10-62333765

† Electronic supplementary information (ESI) available: Powder XRD patterns of the Cu₃(BTC)₂ and SPS–Cu(II)@Cu₃(BTC)₂ nanoparticles. FESEM image of the PS microspheres before sulfonation. Powder XRD patterns and the FESEM photograph of the SPS–Cu(II)@Cu₃(BTC)₂ catalyst after 10 runs of aerobic oxidation of benzyl alcohol under base-free conditions. FESEM photograph of the SPS–Cu(II)@Cu₃(BTC)₂ catalyst after 18 catalytic runs. Powder XRD patterns of the SPS–Cu(II)@CuBDC composite. See DOI: 10.1039/c4ta06046f

without base additives or even under acid conditions. For example, the CuCl/TEMPO catalytic system proposed by Semmelhack *et al.*²⁶ has proven to be highly efficient for catalyzing the selective aerobic oxidation of alcohols under base-free conditions. Cecchetto *et al.*²⁷ found that a Mn(NO₃)₂-Cu(NO₃)₂/TEMPO catalytic system allows the selective oxidation of alcohols to aldehydes and ketones under acid conditions. The formation of oxoammonium cations is believed to be the main mechanism for the actual catalytic oxidation of alcohols in these catalytic systems. Unfortunately, these copper salt catalysts are still homogeneous and are difficult to separate and recycle from the catalytic reaction.

Recently, the proper design and preparation of a controllable active interface between the core and shell in a core-shell structured catalyst has become a fascinating and significant object in nanoscience and nanotechnology.^{28,29} Polymers, as classic substrate materials, can construct a functional surface for efficient heterogeneous catalysts with good dispersity, high stability and easy designability.³⁰ Usually, the catalytically active materials supported on polymer substrates show high catalytic performance,³¹⁻³³ but they often suffer from leaching of active ingredients and poor recyclability during the catalytic reactions.³⁴ To date, the preparation of a stable and efficient heterogeneous catalyst with a controllable active interface is still a challenging research target. It is well known that a porous shell with appropriate mass-transfer channels would be very necessary for a stable catalyst. Metal-organic frameworks (MOFs)³⁵ are of a new class of porous materials consisting of metal/metal clusters and organic ligands. Cu₃BTC₂ (also known as HKUST-1 or CuBTC, BTC = 1,3,5-benzenetricarboxylate) as one of the most widely used MOF materials has received considerable attention in recent years due to its high surface area, tunable pore structures and good chemical stability.³⁶⁻³⁹

In this paper, a novel core-shell SPS-Cu(II)@Cu₃(BTC)₂ catalyst composed of a sulfonated-polystyrene (SPS) core, an active Cu(II) interface and a microporous Cu₃(BTC)₂ shell was developed for catalyzing the aerobic oxidation of alcohols by molecular oxygen under base-free conditions. In the synthetic procedure, Cu(II) ions were first grafted onto a sulfonated-polystyrene core to generate a well-defined active surface decorated with uniform active Cu(II) sites. Part of the -SO₃H grafted copper ions to form the active surface and the rest of the -SO₃H provided acid conditions to produce a high catalytic performance. Moreover, some of the Cu(II) ions linked with the sulfo group further coordinated with H₃BTC ligands to generate a microporous MOF shell. It is noteworthy that the active copper(II) interface, the acid conditions provided by -SO₃H groups on the SPS-Cu(II) surface, and the Cu₃(BTC)₂ shell with uniform porous channels made the catalyst highly efficient for the aerobic oxidation of primary alcohols and it could be recycled 10 times without a significant loss in its catalytic activity. Different SPS-Cu(II)@MOF catalysts such as SPS-Cu(II)@CuBDC were also prepared for catalyzing different catalytic reactions.

2. Experimental section

2.1 Catalyst preparation

Synthesis of the dumbbell-shaped sulfonated-polystyrene (SPS) microspheres. Monodisperse polystyrene (PS) spheres with dumbbell morphology were synthesized *via* seeded emulsion polymerization technology according to the reported procedures.^{40,41} The sulfonated-polystyrene (SPS) template was prepared as follows: 1.0 g of monodisperse PS particles was dispersed in 100 mL concentrated sulfuric acid in a 250 mL three-necked flask equipped with a mechanical stirrer, and the mixed solution was heated to 55 °C and stirred for 6 h. Then the products were separated by centrifugation, washed with ethanol and deionized water, and subsequently dried by lyophilization.

Preparation of the SPS-Cu(II)@Cu₃(BTC)₂ composite. The core-shell structured SPS-Cu(II)@Cu₃(BTC)₂ composite was synthesized according to a facile one-pot procedure. First, the as-prepared SPS spheres (0.1 g) were dispersed in an ethanolic solution of Cu(CH₃COO)₂·H₂O (60 mmol L⁻¹, 10 mL) under magnetic stirring for 5 min at room temperature. The obtained SPS-Cu(II) sample was separated by centrifugation, washed several times with ethanol and then immersed into an ethanolic solution of 1,3,5-benzenetricarboxylic acid (H₃BTC) (20 mmol L⁻¹, 10 mL) at room temperature. After further stirring for about 15 min, the product was collected and washed with ethanol, and the SPS-Cu(II)@Cu₃(BTC)₂ composite was finally obtained.

For catalysis comparison, pure Cu₃(BTC)₂ was synthesized under ambient pressure according to a previously reported method⁴² and its phase purity was confirmed by powder XRD (Fig. S1†). To extend the catalytic system, another novel heterogeneous catalyst of SPS-Cu(II)@CuBDC with a different MOF shell was also synthesized. The synthesis process was the same as that for the SPS-Cu(II)@Cu₃(BTC)₂ nanocomposite, except that 1,4-benzenedicarboxylic acid (H₂BDC) was added into the reaction system instead of H₃BTC.

2.2 Catalytic reaction

The selective oxidation of alcohols was carried out in a 25 mL two-necked flask fitted with a reflux condenser. Typically, certain amounts of catalyst, alcohol (1 mmol) and TEMPO (0.09 mmol) were added to 5 mL of acetonitrile. This system was purged three times with oxygen and then sealed with an O₂ balloon. The reaction mixture was then heated to the desired reaction temperature under stirring. After a required reaction time, the catalysts were removed from the solution by centrifugation and the liquid organic products were analyzed by GC-MS with an HP-5 capillary column by using 1 mmol of nitrobenzene as the internal standard. After each cycle of catalytic reaction, the catalysts were collected by centrifugation, dried at room temperature and then reused in the next run to investigate their recyclability. For the leaching test, the catalytic reaction was stopped after 4 h and the solid catalyst was removed by centrifugation. The reaction solution without the solid catalysts was then stirred for a further 4 h. The catalytic performance in this reaction process was monitored by GC/MS.

To extend the catalytic system, the catalytic performance of SPS-Cu(II)@CuBDC for aerobic oxidation of benzyl alcohol was tested and the reaction conditions were the same as those of SPS-Cu(II)@Cu₃(BTC)₂. Moreover, the catalytic activity of SPS-Cu(II)@CuBDC for aerobic homocoupling of arylboronic acids was also tested and the detailed reaction conditions were as follows: 2 mol% of SPS-Cu(II)@CuBDC catalyst and 2 mmol of phenylboronic acid were stirred in 2 mL of DMF at room temperature for 12 h.

2.3 Characterization

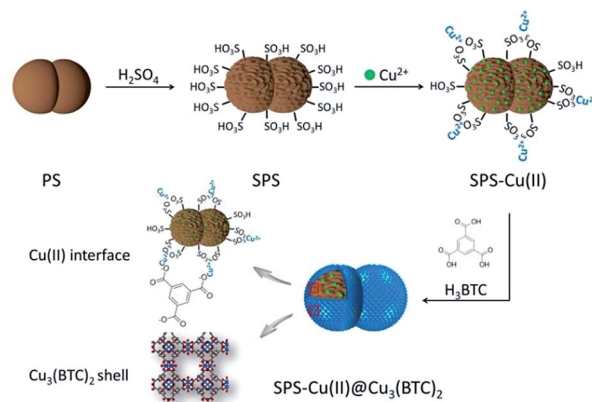
Field-emission scanning electron microscopy (FESEM) images of the products were taken on a ZEISS SUPRA55 instrument with an acceleration voltage of 10 kV. The high-resolution transmission electron microscopy (HRTEM) and high-angle annular dark field scanning transmission electron microscopy (HAADF-STEM) images were recorded on a FEI Tecnai F20 electron microscope operating at 200 kV. Fourier-transform infrared spectra (FTIR) were analyzed using a Nicolet 6700 spectrometer. Powder X-ray diffraction (XRD) patterns of the samples were obtained using a Rigaku D/MAX-RB diffractometer using Cu K α radiation (40 kV, 150 mA, $\lambda = 1.5406 \text{ \AA}$). Copper contents in the products were determined using inductively coupled plasma-atomic emission spectrometry (ICP-AES). Nitrogen adsorption measurements were performed at 77 K on a Quantachrome Autosorb-1. The catalytic efficiency was calculated using a gas chromatography-mass spectrum (Agilent 7890/5975C-GC/MSD).

3. Results and discussion

3.1 Synthesis and characterization

The typical procedure for the synthesis of the SPS-Cu(II)@Cu₃(BTC)₂ composite is shown in Scheme 1. Initially, the dumbbell-like PS particles were treated with concentrated sulphuric acid to generate a functional SO₃H-modified surface and the SPS template was formed. Subsequently, the SPS microspheres were dispersed in an ethanol solution of cupric acetate to attach the copper ions. The functional sulfonic groups introduced into the SPS template had strong affinity for metal cations, which grafted Cu²⁺ ions from the precursor ethanol solution of cupric acetate to form an active Cu(II) interface (SPS-Cu(II)). The Cu₃(BTC)₂ shell, which stabilized and protected the active Cu(II) ions, was generated when the 1,3,5-benzenetricarboxylic acid solution was added to interact with a fraction of the attached Cu²⁺ ions on the surface of the SPS core, and the SPS-Cu(II)@Cu₃(BTC)₂ composite was finally obtained.

The morphology and structure of the SPS and SPS-Cu(II)@Cu₃(BTC)₂ composite were identified by FESEM and HRTEM techniques (Fig. 1). Fig. 1a shows the FESEM image of the as-prepared SPS templates ($\sim 6.3 \mu\text{m}$ length and $\sim 4.1 \mu\text{m}$ diameter) with a uniform dumbbell shape and a pleated surface. Compared to the PS microspheres with a smooth surface (Fig. S2[†]), the wrinkles on the surface of the SPS particles formed during the sulfonation process⁴³ increase the surface area of the polystyrene microspheres, which facilitates the attachment of the active copper ions. Fig. 1b and c show the



Scheme 1 The synthesis process of the SPS-Cu(II)@Cu₃(BTC)₂ composite.

FESEM and HRTEM images of the SPS-Cu(II)@Cu₃(BTC)₂ microspheres with different magnifications. All the SPS microspheres are successfully coated with small Cu₃(BTC)₂ nanocrystals while the dumbbell shape and rough surface of the SPS templates are well maintained (Fig. 1b). The Cu₃(BTC)₂ nanocrystals deposited on the surface of the SPS microsphere exhibit a typical octahedron-like structure with a mean diameter of 80 nm (the inset in Fig. 1b). The HRTEM image in Fig. 1c further reveals that the SPS-Cu(II)@Cu₃(BTC)₂ particles show a core-shell structure with a relatively thin shell composed of fine Cu₃(BTC)₂ nanoparticles and with a shell thickness of about 300 nm. The HAADF-STEM image of a SPS-Cu(II)@Cu₃(BTC)₂ microsphere (Fig. 1d) along with the corresponding elemental mapping of S (Fig. 1e) and Cu (Fig. 1f) in the SPS-Cu(II)@Cu₃(BTC)₂ structure demonstrate that the surface of the polystyrene microsphere is successfully modified with sulfonic acid groups, and the SPS core is uniformly wrapped with the Cu element. The obtained configuration is particularly important

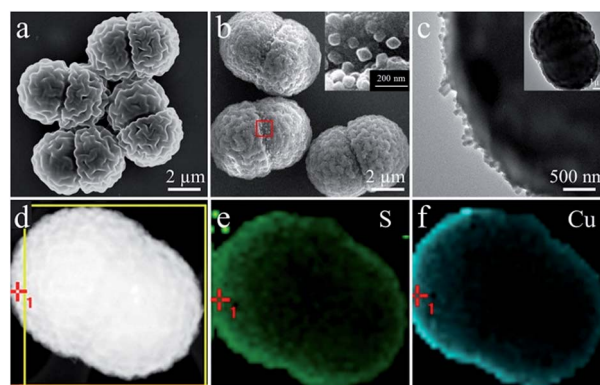


Fig. 1 FESEM images of (a) the SPS template and (b) SPS-Cu(II)@Cu₃(BTC)₂ composite (inset: a high-magnification FESEM image of the Cu₃(BTC)₂ nanoparticles on the surface of the SPS-Cu(II) core); (c) HRTEM image of the SPS-Cu(II)@Cu₃(BTC)₂ particle (inset: a relatively low-magnification HRTEM image of one SPS-Cu(II)@Cu₃(BTC)₂ particle); (d) HAADF-STEM image of an SPS-Cu(II)@Cu₃(BTC)₂ particle and the corresponding elemental mapping of S (e) and Cu (f) in the SPS-Cu(II)@Cu₃(BTC)₂ structure.

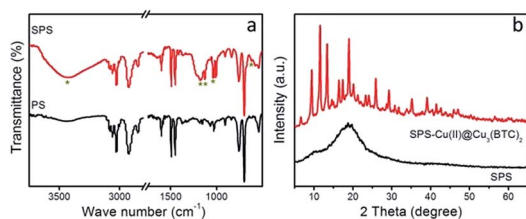


Fig. 2 (a) FTIR spectra of the PS and SPS templates, (b) powder XRD patterns of the SPS template and SPS-Cu(II)@Cu₃(BTC)₂ microspheres.

to achieve a highly efficient catalyst with multiple functions. The free Cu²⁺ ions grafted with the sulfo groups on the surface of the SPS particles aim to gain a robust catalytic activity for the aerobic oxidation of alcohols, and the compact Cu₃(BTC)₂ shell with a porous network structure offers a stable protection layer for the active copper ions as well as appropriate reaction channels to interact with the substrates and reagents.

The successful functionalization of the sulfonic groups is confirmed by FTIR spectroscopy (Fig. 2a). The absorptions at 1038 cm⁻¹, 620 cm⁻¹ and 1181 cm⁻¹ are attributable to the S=O symmetric and asymmetric stretching vibration of the -SO₃H group.^{44,45} The characteristic absorption at 1127 cm⁻¹ is attributable to a sulfonate anion attached to a phenyl ring,⁴⁶ indicating strong bonding interactions between the sulfonic groups and the polystyrene. The crystal structure and chemical composition of the SPS template and SPS-Cu(II)@Cu₃(BTC)₂ composite are further confirmed by powder XRD (Fig. 2b). The broad diffraction peak of the SPS template around 2θ = 20° is attributable to the amorphous PS polymer.⁴⁷ For the SPS-Cu(II)@Cu₃(BTC)₂ microspheres (Fig. 2b), the characteristic diffraction peaks at 2θ values of about 9.52°, 11.68°, 13.46°, 14.61°, 15.01°, 16.49°, 17.50° and 19.08° are assigned to the (220), (222), (400), (331), (420), (422), (333) and (440) planes of Cu₃(BTC)₂ crystals, which is in good agreement with the previous results.^{48,49} No other impurity peaks can be observed. A comparison of the powder diffraction patterns and the unit cell

parameters of Cu₃(BTC)₂ and SPS-Cu(II)@Cu₃(BTC)₂ has been further analysed in the ESI (Fig. S1†).

The porosity of the SPS-Cu(II)@Cu₃(BTC)₂ microspheres is confirmed by nitrogen adsorption-desorption isotherms (Fig. 3). When Cu₃(BTC)₂ nanocrystals are generated on the surface of the SPS-Cu(II) core, the Brunauer-Emmett-Teller (BET) surface area of the SPS-Cu(II)@Cu₃(BTC)₂ composite increases from 3.88 m² g⁻¹ to 227.62 m² g⁻¹, indicating that the porous Cu₃(BTC)₂ shell has been successfully obtained. However, the BET surface area (227.62 m² g⁻¹) and total pore volume (0.37 cm³ g⁻¹) of the SPS-Cu(II)@Cu₃(BTC)₂ composite are much lower than those of the synthesized parent Cu₃(BTC)₂ sample (1112 cm² g⁻¹ and 0.51 cm³ g⁻¹), which may be attributable to the existence of the nonporous SPS-Cu(II) core⁵⁰ or the low synthesis temperature and the short reaction time.⁵¹ The pore diameter of the Cu₃(BTC)₂ calculated by the H-K method is 0.608 nm (the Horváth-Kawazoe (H-K) method was developed for slit pores and has corrections for different pore geometries (cylinder and sphere), and it is a common method for analyzing micropores (<2 nm)). With such a porous shell composed of Cu₃(BTC)₂ nanocrystals, the active Cu(II) interface is well protected and the stability of the SPS-Cu(II)@Cu₃(BTC)₂ catalyst was enhanced.

3.2 Catalytic properties

The selective oxidation of benzyl alcohol to benzaldehyde was chosen as a model reaction to characterize the activity of the SPS-Cu(II)@Cu₃(BTC)₂ catalyst under base-free conditions. The catalytic reaction was carried out at 75 °C using 50 mg of SPS-Cu(II)@Cu₃(BTC)₂ (2 mol% Cu, determined by ICP) as the heterogenous catalyst, 0.09 mmol of TEMPO as the co-catalyst, 1 atm of molecular oxygen as the oxidant and 5 mL of acetonitrile as the solvent. The yield of benzaldehyde *versus* reaction time is shown in Fig. 4. An increase in the yield of benzaldehyde can be observed as the reaction proceeds. Upon reaction for 8 h, the conversion of benzyl alcohol was complete with >99% selectivity (Table 1, entry 1).

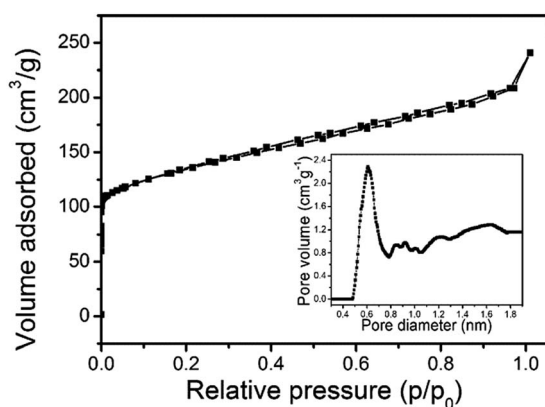


Fig. 3 Nitrogen adsorption-desorption isotherms (inset: pore size distribution) of the SPS-Cu(II)@Cu₃(BTC)₂ composite measured at 77 K.

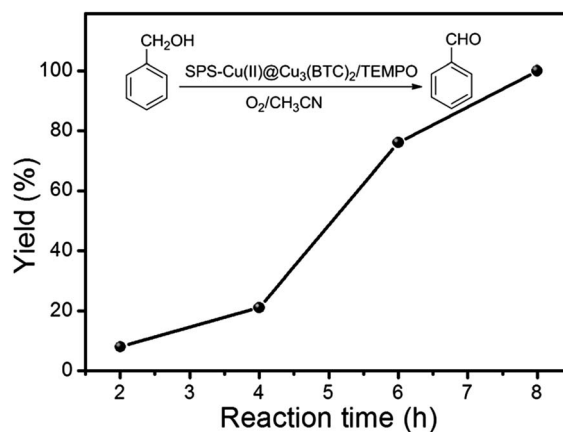


Fig. 4 Yield of benzaldehyde *versus* reaction time catalyzed by the SPS-Cu(II)@Cu₃(BTC)₂ nanocomposite. Reaction conditions: benzyl alcohol (1 mmol), SPS-Cu(II)@Cu₃(BTC)₂ (2 mol%), TEMPO (0.09 mmol), acetonitrile (5 mL), 75 °C, 1 atm O₂ and 1 mmol nitrobenzene.

Table 1 Aerobic oxidation of benzyl alcohol with various catalysts^a

Entry	Catalysts	Time (h)	Yield (%)
1	SPS-Cu(II)@Cu ₃ (BTC) ₂	8	>99
2	—	8	0
3 ^b	SPS	8	0
4	Cu ₃ (BTC) ₂	8	4
5 ^b	SPS + Cu ₃ (BTC) ₂	8	5
6	SPS-Cu(II)	8	>99
7 ^c	SPS-Cu(II)	8	79
8	SPS-Cu(II)@CuBDC	8	>99

^a Reaction conditions: benzyl alcohol (1 mmol), catalyst (2 mol%), TEMPO (0.09 mmol), acetonitrile (5 mL), 75 °C, 1 atm O₂ and 1 mmol nitrobenzene. ^b 50 mg of SPS particles. ^c 0.5 mmol of Na₂CO₃ was added.

To investigate the catalytically active components of the SPS-Cu(II)@Cu₃(BTC)₂ composite, a series of controlled experiments were carried out. The results are summarized in Table 1. Without catalysts (Table 1, entry 2) or just using the SPS template (Table 1, entry 3) as a catalyst, no benzyl alcohol is converted to benzaldehyde. Pure Cu₃(BTC)₂ results in a very low benzaldehyde yield of about 4% (Table 1, entry 4) in the absence of base additives, which agrees with the previous studies.⁵² Trace benzaldehyde is also obtained when using a simple mixture of SPS and Cu₃(BTC)₂ as the catalyst (Table 1, entry 5), suggesting that these two ingredients or the mutual influence between them have almost no catalytic activity for the aerobic oxidation of alcohols under such base-free reaction conditions. When grafting Cu(II) ions onto the SPS surface, the obtained SPS-Cu(II) (Table 1, entry 6) exhibits a benzaldehyde yield of more than 99% after a 8 h reaction time, which is the same as that of the SPS-Cu(II)@Cu₃(BTC)₂ catalyst, indicating that the Cu(II) interface is the main catalytically active component of the SPS-Cu(II)@Cu₃(BTC)₂ catalyst. Interestingly, after adding 0.5 mmol of Na₂CO₃ into the SPS-Cu(II)/TEMPO catalytic system (Table 1, entry 7), the yield of benzaldehyde is reduced to 79%, suggesting that the acid conditions are more favorable for the aerobic oxidation of benzyl alcohol in this catalytic system. These results are in conformity with the previously reported catalytic mechanism,⁵³⁻⁵⁶ in which the oxoammonium cations formed from the synergy of the Cu(II) interface and TEMPO played a key role in the oxidation of alcohols.

In order to verify the effect of the Cu₃(BTC)₂ shell on stabilizing the active Cu(II) interface, the recyclability of the SPS-Cu(II) and SPS-Cu(II)@Cu₃(BTC)₂ catalysts was examined for the selective oxidation of benzyl alcohol. After each reaction cycle, the catalysts were separated by centrifugation, dried at room temperature, and then reused for a consecutive run under the same reaction conditions. Fig. 5 shows that the SPS-Cu(II)@Cu₃(BTC)₂ catalyst remains substantially active for over 10

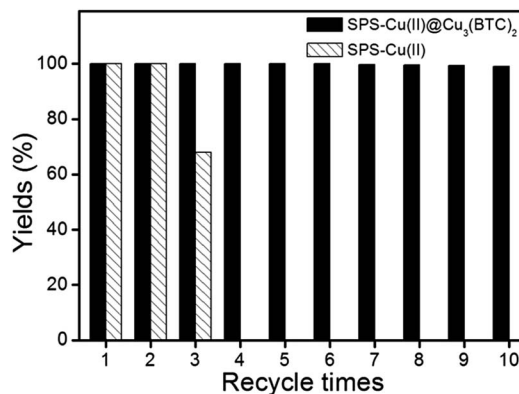


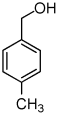
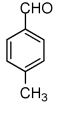
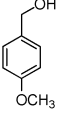
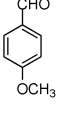
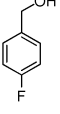
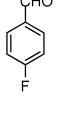
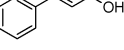
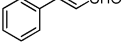
Fig. 5 Recycling results for selective oxidation of benzyl alcohol to benzaldehyde. Reaction conditions: benzyl alcohol (1 mmol), catalyst (2 mol%), TEMPO (0.09 mmol), acetonitrile (5 mL), 75 °C, 8 h, 1 atm O₂ and 1 mmol nitrobenzene.

recycles, and the yield of benzaldehyde was 99.1% after ten runs. The powder XRD patterns (Fig. S3†) and FESEM images (Fig. S4†) of the catalyst after 10 cycles show that the overall structure of the material remains intact after the catalytic experiments, indicating that the SPS-Cu(II)@Cu₃(BTC)₂ catalyst is quite stable under the base-free reaction conditions. After 11 cycles, the conversion of benzyl alcohol decreased from 99.1% (after 10 cycles) to 86.4% (after 11 cycles) with the selectivity of benzaldehyde more than 99% and the structure of the catalyst were well maintained. After 18 cycles, the structure of the SPS-Cu(II)@Cu₃(BTC)₂ composite was broken (Fig. S5†). In contrast, in the case of the SPS-Cu(II) sample (Fig. 5), the benzaldehyde yield decreases significantly to 68% after only three cycles.

The metal leaching tests were also carried out to further verify the stability of the SPS-Cu(II) and SPS-Cu(II)@Cu₃(BTC)₂ catalysts, in which the solid catalyst was centrifuged and removed after 4 h and the reaction continued. The results showed that after the removal of the SPS-Cu(II) catalyst, the yield of benzaldehyde increased from 23% to 65% during the next 4 h after centrifugation, indicating obvious copper leaching in the catalytic reaction. However, in the case of the SPS-Cu(II)@Cu₃(BTC)₂ catalyst, the yield of benzaldehyde was 21% in the first 4 h, and no further conversion of benzyl alcohol could be observed when the reaction continued for another 4 h without the solid catalyst, suggesting that the porous Cu₃(BTC)₂ shell efficiently protected the heterogenous catalyst from metal leaching as well as provided mass transfer channels during the catalytic reaction.

To sum up, the SPS-Cu(II)@Cu₃(BTC)₂ catalyst with such a well-designed structure exhibited excellent catalytic activity, high stability and good recyclability. It is also important to emphasize that the sulfonation treatment of the SPS microspheres was designed to graft Cu²⁺ ions to form the active Cu(II) interface as well as provide acid conditions for high catalytic efficiency. The attached Cu²⁺ ions also played a dual role in the formation of the SPS-Cu(II)@Cu₃(BTC)₂ core-shell structures. Firstly, the copper ions as the active sites produced high

Table 2 Selective oxidation of various alcohol substrates using the SPS-Cu(II)@Cu₃(BTC)₂ catalyst with molecular oxygen^a

Entry	Substrates	Products	Time (h)	Yield (%)	Selectivity (%)
1			8	>99	>99
2			10	>99	>99
3			9	82	>99
4			12	>99	>99
5			9	>99	>99
6			11	>99	>99
7			8	3	>99
8			8	3	>99
9			8	4	>99

^a Reaction conditions: alcohol (1 mmol), SPS-Cu(II)@Cu₃(BTC)₂ (2 mol% Cu), TEMPO (0.09 mmol), acetonitrile (5 mL), 75 °C, 1 atm O₂ and 1 mmol nitrobenzene.

catalytic efficiency. Furthermore, as one of the most important starting materials, the Cu²⁺ ions initiated the nucleation of the Cu₃(BTC)₂ nanocrystals. The MOF shells stabilized the linkage between the copper ions and the sulfo groups on the surface of the SPS template, which enhanced the catalytic recyclability. Moreover, the porous Cu₃(BTC)₂ shell provided uniform pore channels to accelerate the mass transfer in the catalytic reaction process and further improved the catalytic performance of the SPS-Cu(II)@Cu₃(BTC)₂ catalyst.

To explore the scope of the novel catalytic system, the catalytic activities of the SPS-Cu(II)@Cu₃(BTC)₂ composite assisted by TEMPO as the co-catalyst for the selective oxidation of various alcohol substrates were also tested under the same conditions. The catalytic results are summarized in Table 2. It can be observed that the corresponding carbonyl compounds are the sole detectable products under such base-free reaction conditions. Specifically, *p*-substituted benzylic alcohols such as *p*-methylbenzyl (Table 2, entry 1), *p*-methoxy benzyl alcohols (Table 2, entry 2) and 4-fluorobenzyl alcohol (Table 2, entry 3) all

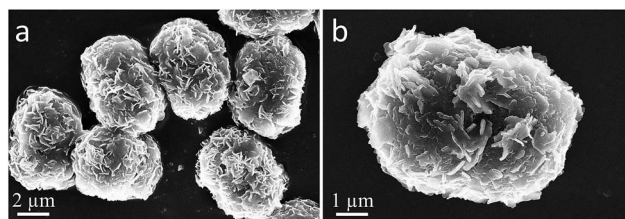


Fig. 6 FESEM images of the SPS-Cu(II)@CuBDC composite under different magnifications.

show 100% conversion to their corresponding aldehydes after a required reaction time. Aerobic oxidation of heterocyclic alcohol such as pyridin-2-yl-methanol (Table 2, entry 4) exhibits excellent pyridine-2-carboxaldehyde yield (>99%) as well. The allylic alcohol reactions also confirm that both cinnamyl alcohol (Table 2, entry 5) and 3-methyl-2-buten-1-ol (Table 2, entry 6) result in complete conversion with >99% selectivity of the corresponding aldehydes without disturbing their C=C double bonds. However, secondary alcohols such as 1-phenylethanol, 2-cyclohexen-1-ol and cyclopentanol (Table 2, entries 7–9) are difficult to oxidize to their corresponding ketones in the present protocol, which is probably due to steric interactions.^{1,7} The scope of the aerobic oxidation can be extended by simply adjusting the copper component or just changing the reaction conditions. The SPS-Cu(II)@Cu₃(BTC)₂ catalyst performance is well consistent with that of copper salt catalysts,^{26,27} further indicating that Cu(II) is the main active component of the SPS-Cu(II)@Cu₃(BTC)₂ catalyst.

Different MOF shells can be easily prepared to form a variety of SPS-Cu(II)@MOF catalysts. For example, a novel dumbbell-shaped SPS-Cu(II)@CuBDC composite with a laminated CuBDC shell (Fig. 6) was synthesized. The characteristics of CuBDC were confirmed by powder XRD (Fig. S6†). The catalytic activity of SPS-Cu(II)@CuBDC (Table 1, entry 8) for the aerobic oxidation of benzyl alcohol under the same conditions is comparable to that of the SPS-Cu(II)@Cu₃(BTC)₂ composite, owing to the existence of the effective mass transfer channels provided by the porous structure of CuBDC and the interstices among the adjacent CuBDC nanosheets. The results also confirmed that the Cu(II) interface between the SPS core and the MOF shell was the active component of the SPS-Cu(II)@MOF catalyst. To extend the catalytic system, the obtained SPS-Cu(II)@CuBDC composite was used to catalyse aerobic homocoupling of phenylboronic acid to biphenyl at room temperature, and high catalytic activity (85% conversion, 100% selectivity) was achieved after reaction for 12 h, indicating that the multifunctional structure of the SPS-Cu(II)@MOF catalyst can be applied for different catalytic reactions with high efficiency.

4. Conclusions

In summary, a novel heterogeneous core-shell SPS-Cu(II)@Cu₃(BTC)₂ catalyst with a controllable active Cu(II) interface was fabricated *via* a facile method under mild synthesis conditions. The active Cu(II) interface generated by attaching

Cu²⁺ ions with –SO₃H groups on the surface of the SPS cores was the main active component of the SPS–Cu(II)@Cu₃(BTC)₂ catalyst. The excess –SO₃H groups provided acid conditions to enhance the catalytic efficiency. The porous Cu₃(BTC)₂ shell formed by the coordination between a portion of Cu(II) ions and H₃BTC ligands acted as a protective layer to avoid the leaching of active Cu²⁺ ions and also provided uniform microchannels for mass transfer. The active Cu(II) interface, the excess –SO₃H groups and the porous Cu₃(BTC)₂ shell made the SPS–Cu(II)@Cu₃(BTC)₂ composite an excellent catalyst with high efficiency and reusability for the aerobic oxidation of alcohols to aldehydes under base-free conditions. The conversion of benzyl alcohol was 100% with >99% benzaldehyde selectivity. The SPS–Cu(II)@Cu₃(BTC)₂ catalyst could be recycled ten times without a significant loss in its activity and selectivity. Furthermore, a novel SPS–Cu(II)@CuBDC catalyst with a laminated CuBDC shell was also synthesized, and exhibited favorable catalytic properties for the aerobic oxidation of alcohols as well as for the catalytic reaction of the aerobic homocoupling of arylboronic acids. Therefore the controllable design of the SPS–Cu(II)@MOF structure provides a general approach for the exploration of highly efficient and stable heterogeneous catalysts for different catalytic reaction systems.

Acknowledgements

We would like to thank the National High Technology Research and the Development Program of China (863 Program) (no. 2013AA031702) and the Co-building Special Project of Beijing Municipal Education for their support.

Notes and references

- R. H. Liu, X. M. Liang, C. Y. Dong and X. Q. Hu, *J. Am. Chem. Soc.*, 2004, **126**, 4112–4113.
- R. F. Nie, J. J. Shi, W. C. Du, W. S. Ning, Z. Y. Hou and F. S. Xiao, *J. Mater. Chem. A*, 2013, **1**, 9037–9045.
- S. J. Liu, N. Zhang, Z. R. Tang and Y. J. Xu, *ACS Appl. Mater. Interfaces*, 2012, **4**, 6378–6385.
- M. B. Lauber and S. S. Stahl, *ACS Catal.*, 2013, **3**, 2612–2616.
- M. Shibuya, Y. Osada, Y. Sasano, M. Tomizawa and Y. Iwabuchi, *J. Am. Chem. Soc.*, 2011, **133**, 6497–6500.
- K. Yamaguchi and N. Mizuno, *Angew. Chem., Int. Ed.*, 2002, **41**, 4538–4542.
- J. L. Long, X. Q. Xie, J. Xu, Q. Gu, L. M. Chen and X. X. Wang, *ACS Catal.*, 2012, **2**, 622–631.
- A. Rahimi, A. Azarpira, H. Kim, J. Ralph and S. S. Stahl, *J. Am. Chem. Soc.*, 2013, **135**, 6415–6418.
- C. Parmeggiani and F. Cardona, *Green Chem.*, 2012, **14**, 547–564.
- M. L. Kantam, R. S. Reddy, K. Srinivas, R. Chakravarti, B. Sreedhar, F. Figuera and C. V. Reddy, *J. Mol. Catal. A: Chem.*, 2012, **355**, 96–101.
- Y. H. Kim, S. K. Hwang, J. W. Kim and Y. S. Lee, *Ind. Eng. Chem. Res.*, 2014, **53**, 12548–12552.
- S. Venkatesan, A. S. Kumar, J. F. Lee, T. S. Chan and J. M. Zen, *Chem. Commun.*, 2009, 1912–1914.
- H. L. Liu, Y. L. Liu, Y. W. Li, Z. Y. Tang and H. F. Jiang, *J. Phys. Chem. C*, 2010, **114**, 13362–13369.
- S. E. Allen, R. R. Walvoord, R. P. Salinas and M. C. Kozlowski, *Chem. Rev.*, 2013, **113**, 6234–6458.
- S. Pande, A. Saha, S. Jana, S. Sarkar, M. Basu, M. Pradhan, A. K. Sinha, S. Saha, A. Pal and T. Pal, *Org. Lett.*, 2008, **10**, 5179–5181.
- E. T. T. Kumpulainen and A. M. P. Koskinen, *Chem.–Eur. J.*, 2009, **15**, 10901–10911.
- K. T. Mahmudov, M. N. Kopylovich, M. Silva, P. J. Figiel, Y. Y. Karabach and A. J. L. Pombeiro, *J. Mol. Catal. A: Chem.*, 2010, **318**, 44–50.
- P. Gamez, I. W. C. E. Arends, J. Reedijk and R. A. Sheldon, *Chem. Commun.*, 2003, 2414–2415.
- P. J. Figiel, A. Sibaouih, J. U. Ahmad, M. Nieger, M. T. Räisänen, M. Leskelä and T. Repo, *Adv. Synth. Catal.*, 2009, **351**, 2625–2632.
- Q. F. Wang, Y. Zhang, G. X. Zheng, Z. Z. Tian and G. Y. Yang, *Catal. Commun.*, 2011, **14**, 92–95.
- Z. L. Lu, T. Ladrak, O. Roubeau, J. van der Toorn, S. J. Teat, C. Massera, P. Gamez and J. Reedijk, *Dalton Trans.*, 2009, 3559–3570.
- P. J. Figiel, A. M. Kirillov, M. F. C. Guedes da Silva, J. Lasri and A. J. L. Pombeiro, *Dalton Trans.*, 2010, **39**, 9879–9888.
- H. Chen, Q. H. Tang, Y. T. Chen, Y. B. Yan, C. M. Zhou, Z. Guo, X. L. Jia and Y. H. Yang, *Catal. Sci. Technol.*, 2013, **3**, 328–338.
- H. Miyamura, R. Matsubara, Y. Miyazaki and S. Kobayashi, *Angew. Chem., Int. Ed.*, 2007, **46**, 4151–4154.
- N. F. Zheng and G. D. Stucky, *Chem. Commun.*, 2007, 3862–3864.
- M. F. Semmelhack, C. R. Schmid, D. A. Cortés and C. S. Chou, *J. Am. Chem. Soc.*, 1984, **106**, 3374–3376.
- A. Cecchetto, F. Fontana, F. Minisci and F. Recupero, *Tetrahedron Lett.*, 2001, **42**, 6651–6653.
- X. W. Zhang, G. Wang, M. Yang, Y. Luan, W. J. Dong, R. Dang, H. Y. Gao and J. Yu, *Catal. Sci. Technol.*, 2014, **4**, 3082–3089.
- Y. H. Deng, Y. Cai, Z. K. Sun, J. Liu, C. Liu, J. Wei, W. Li, C. Liu, Y. Wang and D. Y. Zhao, *J. Am. Chem. Soc.*, 2010, **132**, 8466–8473.
- X. B. Huang, W. C. Guo, G. Wang, M. Yang, Q. Wang, X. X. Zhang, Y. H. Feng, Z. Shi and C. G. Li, *Mater. Chem. Phys.*, 2012, **135**, 985–990.
- G. Grivani, S. Tangestaninejad, M. H. Habibi and V. Mirkhani, *Catal. Commun.*, 2005, **6**, 375–378.
- G. Pozzi, M. Cavazzini, S. Quici, M. Benaglia and G. Dell'Anna, *Org. Lett.*, 2004, **6**, 441–443.
- M. Gilhespy, M. Lok and X. Baucherel, *Chem. Commun.*, 2005, 1085–1086.
- A. Dijksman, I. W. C. E. Arends and R. A. Sheldon, *Chem. Commun.*, 2000, 271–272.
- Y. F. Zhang, X. G. Bo, A. Nsabimana, C. Han, M. Li and L. P. Guo, *J. Mater. Chem. A*, 2015, **3**, 732–738.
- S. S. Y. Chui, S. M. F. Lo, J. P. H. Charmant, A. G. Orpen and L. D. A. Williams, *Science*, 1999, **283**, 1148–1150.

- 37 L. D. O'Neill, H. Zhang and D. Bradshaw, *J. Mater. Chem.*, 2010, **20**, 5720–5726.
- 38 M. G. Schwab, I. Senkowska, M. Rose, M. Koch, J. Pahnke, G. Jonschker and S. Kaskel, *Adv. Eng. Mater.*, 2008, **10**, 1151–1155.
- 39 D. Bradshaw, A. Garai and J. Huo, *Chem. Soc. Rev.*, 2012, **41**, 2344–2381.
- 40 H. R. Sheu, M. S. El-Aasser and J. W. Vanderhoff, *J. Polym. Sci., Part A: Polym. Chem.*, 1990, **28**, 629–651.
- 41 H. R. Sheu, M. S. El-Aasser and J. W. Vanderhoff, *J. Polym. Sci., Part A: Polym. Chem.*, 1990, **28**, 653–667.
- 42 M. Hartmann, S. Kunz, D. Himsl and O. Tagermann, *Langmuir*, 2008, **24**, 8634–8642.
- 43 M. Z. Wang, X. P. Ge, H. Wang, Q. Yuan, X. W. Ge, H. R. Liu and T. Tang, *Langmuir*, 2010, **26**, 1635–1641.
- 44 Z. Z. Yang, Z. W. Niu, Y. F. Lu, Z. B. Hu and C. C. Han, *Angew. Chem., Int. Ed.*, 2003, **42**, 1943–1945.
- 45 F. Kucera and J. Jancar, *Polym. Eng. Sci.*, 1998, **38**, 783–792.
- 46 R. A. Weiss, S. Ashish, C. L. Willis and L. A. Pottick, *Polymer*, 1991, **32**, 1867–1874.
- 47 C. R. Martins, G. Ruggeri and M. de Paoli, *J. Braz. Chem. Soc.*, 2003, **14**, 797–802.
- 48 P. Chowdhury, C. Bikkina, D. Meister, F. Dreisbach and S. Gumma, *Microporous Mesoporous Mater.*, 2009, **117**, 406–413.
- 49 B. Panella, M. Hirscher, H. Pütter and U. Müller, *Adv. Funct. Mater.*, 2006, **16**, 520–524.
- 50 F. Ke, L. G. Qiu and J. F. Zhu, *Nanoscale*, 2014, **6**, 1596–1601.
- 51 A. L. Li, F. Ke, L. G. Qiu, X. Jiang, Y. M. Wang and X. Y. Tian, *CrystEngComm*, 2013, **15**, 3554–3559.
- 52 A. Dhakshinamoorthy, M. Alvaro and H. Garcia, *ACS Catal.*, 2011, **1**, 48–53.
- 53 W. Schiff, L. Stefaniak, J. Skolimowski and G. A. Webb, *J. Mol. Struct.*, 1997, **407**, 1–3.
- 54 A. E. J. de Nooy, A. C. Besemer and H. van Bekkum, *Synthesis*, 1996, **10**, 1153–1176.
- 55 P. J. Figiel, M. Leskelä and T. Repo, *Adv. Synth. Catal.*, 2007, **349**, 1173–1179.
- 56 P. Gamez, I. W. C. E. Arends, R. A. Sheldon and J. Reedijk, *Adv. Synth. Catal.*, 2004, **346**, 805–811.